Hindawi
Complexity
Volume 2018, Article ID 9432897, 14 pages
https://doi.org/10.1155/2018/9432897

Research Article

FDM Rapid Prototyping Technology of Complex-Shaped Mould Based on Big Data Management of Cloud Manufacturing

Yan Cao, Liang Huang, Yu Bai, and Qingming Fan

School of Mechatronic Engineering, Xi'an Technological University, Xi'an 710021, China

Correspondence should be addressed to Yan Cao; jantonyz@163.com

Received 13 July 2018; Revised 30 August 2018; Accepted 9 September 2018; Published 1 November 2018

Guest Editor: Zhihan Lv

In order to solve the problem of high cost and long cycle in the process of traditional subtractive material manufacturing of a complex-shaped mould, the technology of FDM rapid prototyping is used in combination with the global service idea of cloud manufacturing, where the information of various kinds of heterogeneous-forming process data produced in the process of FDM rapid prototyping is analysed. Meanwhile, the transfer and transformation relation of each forming process data information in the rapid manufacturing process with the digital model as the core is clarified, so that the FDM rapid manufacturing process is integrated into one, thus forming a digital and intelligent manufacturing system for a complex-shaped mould based on the cloud manufacturing big data management. This paper takes the investment casting mould of a spur gear as an example. Through research on the forming mechanism of jet wire, the factors affecting forming quality and efficiency is analysed from three stages: the pretreatment of the 3D model, the rapid prototyping, and the postprocessing of the forming parts. The relationship between the forming parameters and the craft quality is thus established, and the optimization schemes at each stage of this process are put forward through the study on the forming mechanism of jet wire. Through a rapid prototyping test, it is shown that the spur face gear master mould based on this technology can be quickly manufactured with a critical surface accuracy within a range of 0.036 mm–0.181 mm and a surface roughness within the range of 0.007–0.01 μm by only 1/3 the processing cycle of traditional subtractive material manufacturing. It lays a solid foundation for rapid intelligent manufacturing of products with a complex-shaped structure.

1. Introduction

As a modern process equipment, the mould has been widely used in industrial production with its high precision, high complexity, and high consistency products. However, the way of manufacturing using a mould has been a technology bottleneck that has not yet found a breakthrough. This is especially true for the complex-shaped mould. The subtractive material manufacturing does not only have a long processing cycle and high processing costs, but the consistency of the products is hard to guarantee due to the constraints of the processing machinery itself. With the development and application of the additive material manufacturing technology in recent years, the rapid prototyping mould method appeared (RT technology) [1–3]. This technology integrates the rapid prototyping technology with the traditional non-machining cavity replication technology. Compared with the traditional subtractive material manufacturing method, the rapid manufacturing of a complex-shaped mould can be accomplished with only one third of the traditional processing cycle and processing cost. It can realize the rapid production of a small batch of the complex-shaped products by docking the technology with the investment casting.

Since the FDM rapid prototyping technology is the only high quality rapid prototyping method at present with industrial grade thermoplastic material as the forming material [4], it is suitable for the production of an investment casting mould. However, in the rapid prototyping process, with the development of forming technology research, a large number of heterogeneous-forming process data information related to the quality and efficiency of the forming process will be produced. Furthermore, these sources of information are also related to each other. Therefore, how to extract, sum up, and utilize the forming process big data produced in

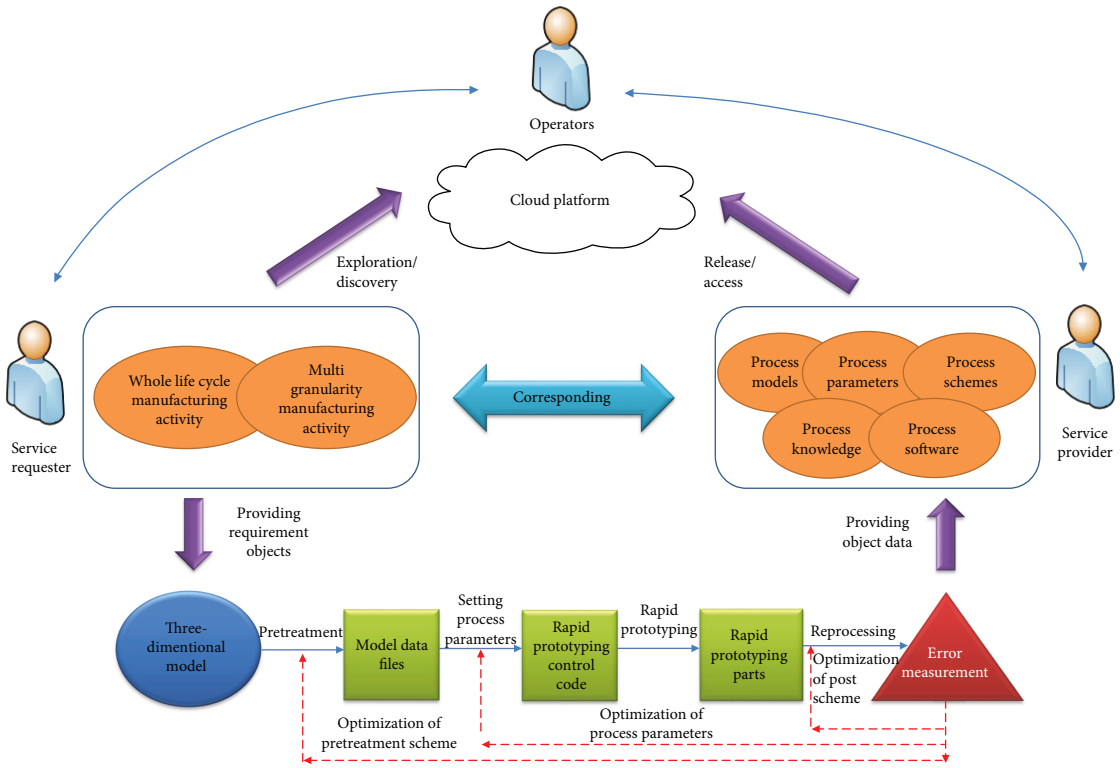

FIGURE 1: The intelligent manufacturing system of the FDM rapid prototyping complex-shaped mould based on the big data management of cloud manufacturing.

the above forming process has become a research hotspot of advanced manufacturing technology under the background of the information age [5–7]. In order to adapt to the complex and changeable market demand, a new networked manufacturing model based on the integration of information technology and manufacturing industry has emerged—-cloud manufacturing [8, 9]. Cloud manufacturing provides a new network manufacturing model for users with various types of on-demand manufacturing services. The architecture of cloud manufacturing integration is a set of models describing the integration of cloud manufacturing functions, including functional definitions, interface rules, and architecture. These models describe how the cloud manufacturing platform forms a loosely coupled distributed environment, including the functional structure, characteristics, and operation mode. So, in the rapid prototyping process, these so-called "forming processes big data" will take the digital model as the core to transfer and transform in the manufacturing process and ultimately directly affect the processing quality and efficiency. Typical work, such as that of Professor D. Li, proposes a cloud manufacturing network model for workshop manufacturing [10]. Combined with the intelligent evaluation and control algorithm of big data feedback, the accuracy of the workshop cloud manufacturing network model was improved. Meanwhile, a cloud manufacturing process model for hydrostatic systems based on manufacturing big data was proposed by Z. F. Liu, and the intelligent manufacturing process was realized by combining the cloud service platform [11].

Based on the above analysis, combined with the cloud manufacturing service concept [12], by taking big data as the main processing basis, the paper studies the internal relationship between data and the mechanism of data acting on product demand, and constructs a network of data function coordination relations. The big data produced in the miscellaneous manufacturing process is organized effectively, so that the intelligent and efficient rapid manufacturing of complex products can be realized by the manufacturing system based on the cloud manufacturing big data management. Therefore, this paper takes the investment casting mould of a spur gear as an example (that is, the master mould of a spur face gear), starting with the material-forming mechanism of the FDM rapid prototyping technology, and studies the various stages of the rapid prototyping of a spur face gear master mould. By analysing the influence of the process information data in each stage on the forming accuracy and efficiency, as well as the research on the change of the wire during the forming process, from the angle of reducing the surface roughness and improving the forming precision, the expression relationship between the information data of rapid prototyping and the forming quality is established. Based on this expression, the reasonable selection method of forming process parameters is determined. Finally, the theoretical model of the process system is constructed by using the moulding process big data obtained by the process, and connected with the cloud manufacturing technology. Thus, the intelligent manufacturing system of the FDM rapid prototyping complex-shaped mould based on the big data management

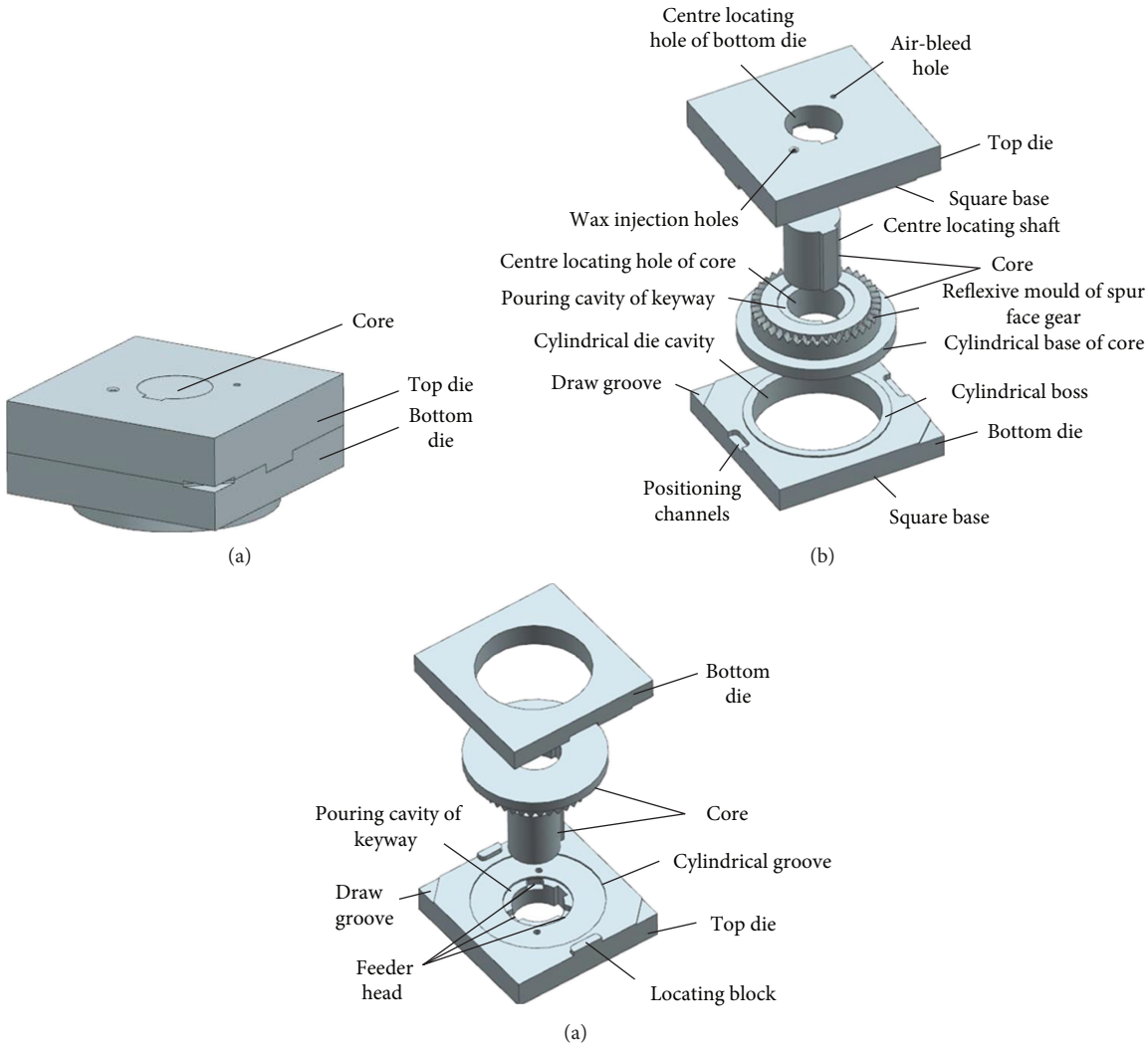

Figure 2: Sketch of the spur face gear master mould.

of cloud manufacturing is realized (the flow chart is shown in Figure 1).

2. Analysis of the Spur Face Gear Master Mould Structure

Considering that the master mould of a spur face gear is mainly used as a wax injection mould in the investment casting process and that this mould has the problem of poor thermal conductivity when FDM rapid prototyping technology is used to manufacture a mould with thermoplastic material, in order to remove the master mould conveniently without affecting the precision of the wax mould, the master mould of the spur face gear is designed by UG software as a three-layer structure consisting of a top die, a bottom die, and a core with a movable centre-locating shaft according to the injection mould design method with movable parts [13, 14] (as shown in Figure 2, the top die and the bottom die are moving dies, and the core is a static die).

Table 1: The performance parameters of ABS materials.

Materials	Tensile strength	Ultimate tensile ratio
ABS	≥43 Mpa	4%
Melting temperature	Distortion temperature	Linear shrinkage
200°C–250°C	93°C–118°C	0.4%
Bending strength	Impact strength	Coefficient of linear expansion
790 kg/cm^2	20 kJ/m^2	7×10^{-5}/°C

3. Process Big Data Analysis of Rapid Prototyping Spur Face Gear Master Mould Based on FDM

According to the investment casting process requirements on the use of a wax injection mould material with high temperature performance, hardness, and strength, as well as having

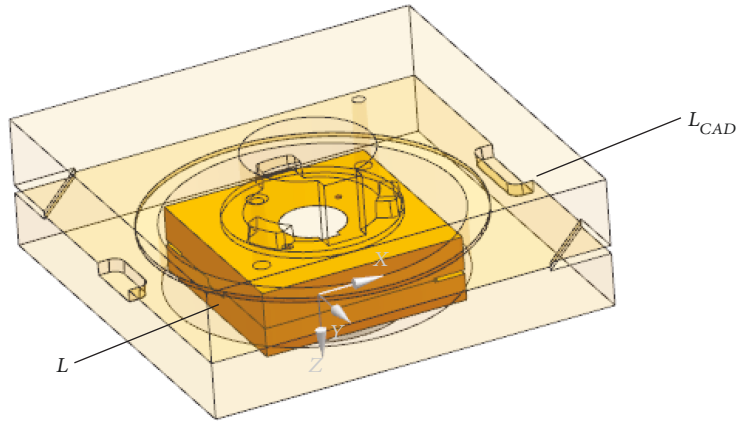

Figure 3: Sketch of rapid prototyping shrinkage for the spur face gear master mould.

Table 2: The shrinkage percentage of each spur face gear master mould.

		Core		
Cylindrical base	Reflexive mould of spur face gear	Pouring cavity of keyway	Centre-locating hole of core	Centre-locating shaft
1.12%	0.22%	0.35%	0.51%	0.64%
Bottom die				
Square base			Cylindrical boss	
1.46%			0.19%	
Top die				
Square base	Cylindrical groove	Pouring cavity of keyway	Centre-locating hole of core	
1.41%	0.10%	0.41%	0.57%	

characteristics of low viscosity, low shrinkage necessary, and good bonding ability for thermoplastic materials used in FDM rapid prototyping technology [15, 16], the forming material selected is ABS. The performance parameters of ABS materials are shown in Table 1, and the corresponding rapid prototyping equipment is the BOX 3D rapid prototyping machine provided by Beijing Lingyang Aipu Technology Co. Ltd.

3.1. Analysis of Process Parameters of Spur Face Gear Master Mould in the Preprocessing Stage of Rapid Prototyping. Firstly, before adopting the FDM rapid prototyping technology to produce the master mould of the spur face gear, some factors need to be considered; for example, ABS is a thermoplastic material that causes the dimensions of the forming parts to shrink during the forming process and the shrinkage of each forming part is carried out in different directions [17]. Thus, there are some relationships between the size shrinkage of each forming part S_L, the corresponding 3D model size L_{CAD}, and the actual size of the moulded part L that are shown in Figure 3.

$$S_L = \frac{(L_{CAD} - L)}{L_{CAD}}, \quad (1)$$

where L_{CAD} is the three-dimensional model of the spur face gear master mould and L is the actual part of spur face gear master mould.

Therefore, according to (1), the shrinkage percentage of each mould part can be calculated through a rapid prototyping test (as shown in Table 2). Furthermore, according to the shrinkage percentage of each mould part shown in Table 2, the original 3D model of the spur face gear master mould is enlarged by using UG software.

Secondly, the three-dimensional model of the enlarged spur face gear master mould is used for the extraction of the shell. Because of proper shell disposal, the manufacturing cost can be reduced and the forming speed can be improved on the basis of not affecting the original performance of the master mould (including the high temperature performance, strength, and hardness). Furthermore, the distortion and cracking of the mould surface can also be prevented. In order to determine the influence of different shell thicknesses on the quality and performance of the mould parts, simulation experiments of shell extraction and wax injection are carried out for 6 different shell thicknesses in Figure 3 by adopting the control variety method. According to the experimental results shown in Table 3, a reasonable shell thickness of 0.8 mm is selected for the master mould taking into account both forming efficiency and manufacturing cost.

Table 3: Setting of the shell thickness.

Sequence number	1	2	3	4	5	6
Shell thickness (mm)	1.0	0.9	0.8	0.7	0.6	0.5
Experimental result	Normal	Normal	Normal	Warp and distortion	Warp and distortion seriously	Deformation

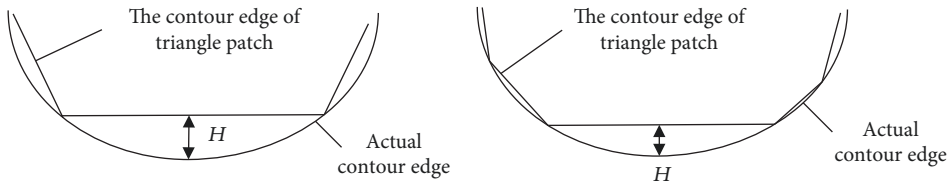

(a) The fitting precision of model is low when the chord deviation is larger

(b) The fitting precision of the model is high when the chord deviation is smaller

Figure 4: Effect of different chord deviations on the accuracy of the STL model.

Table 4: The most optimized parameter setting method for converting the STL model.

UG
(1) File → export → STL → the setting type is binary
(2) The triangle tolerance is 0.0025
(3) The adjacent tolerance is 0.12
(4) Open automatic normal generation
(5) Close normal indication
(6) Open triangle indication

The model data of the master mould must be converted into the data format that can be recognized by the RP equipment after finishing the optimization of the 3D model of the spur face gear master mould, because the forming process parameters are set up on the basis of the imported model data. The mainstream data format that can be identified by the current rapid prototyping machine is STL [18, 19]. The essence of the STL data format is to use hundreds of tiny triangular patches to replace a curved surface, thus reconstructing the original 3D model. The error of the STL model is controlled by the chord deviation H (as shown in Figure 4). If you get the high precision STL model by increasing the number of triangles, it will not only exceed the maximum forming accuracy that FDM can achieve, but it will also increase the data storage during the STL model data slicing process. Therefore, it is important to find a balance point between forming precision and forming efficiency.

At present, the most optimized parameter setting method for converting the STL model by using UG software is shown in Table 4, and by this method, the STL model of the spur face gear master mould can be obtained (as shown in Figure 5).

3.2. Analysis of Forming Process Parameters of Spur Face Gear Master Mould in the Processing Stage of Rapid Prototyping. Although many factors have more or less influence on forming efficiency and forming quality (including dimensional accuracy and surface roughness) in the FDM rapid prototyping process, it is mainly controlled by seven important technological parameters, which are the thickness of the layer and the forming direction, the extrusion speed and filling speed, the nozzle temperature and the ambient temperature, and the compensation of the ideal contour line [20–22].

3.2.1. Selection of Layer Thickness and Forming Direction. The layer thickness is the slice thickness of the three-dimensional model, and it is also the manufacturing height of each layer of the FDM rapid prototyping machine for laminated object manufacturing. The forming direction refers to the spatial arrangement of forming parts in the forming process. Since the manufacturing method of the FDM rapid prototyping technology is superimposed layer by layer, the contour of each slice is inconsistent and has a certain thickness during formation [23]. As a result, the surface of the moulded parts often exhibits a "Step Effect" (as shown in Figure 6), which would further affect the quality of the moulded parts. At present, the technical indexes of the "Step Effect" in the FDM rapid prototyping process are mainly ε and δ, where ε reflects the shape error of the moulded part, and δ reflects the roughness of the moulded part. According to the geometric relationship shown in Figure 6, the relation between the layer thickness h and forming direction α, ε, and δ can be concluded, respectively.

$$\varepsilon = R\left[\cos\alpha - \sqrt{1 - \left(\sin\alpha + \frac{h}{R}\right)^2}\right], \tag{2}$$

$$\delta = R\left[1 - \sqrt{1 - \frac{2h\sin\alpha}{R} - \left(\frac{h}{R}\right)^2}\right]. \tag{3}$$

To investigate the influence of different slice heights and forming directions on the surface of the moulded parts ε and δ, taking the hemisphere model of $R = 100$ mm as an example, the corresponding relation curve is plotted by Matlab in accordance with (2) and (3) (as shown in Figure 7).

According to Figure 7, the larger the h value is, the greater the ε value and δ value on the surface of moulded

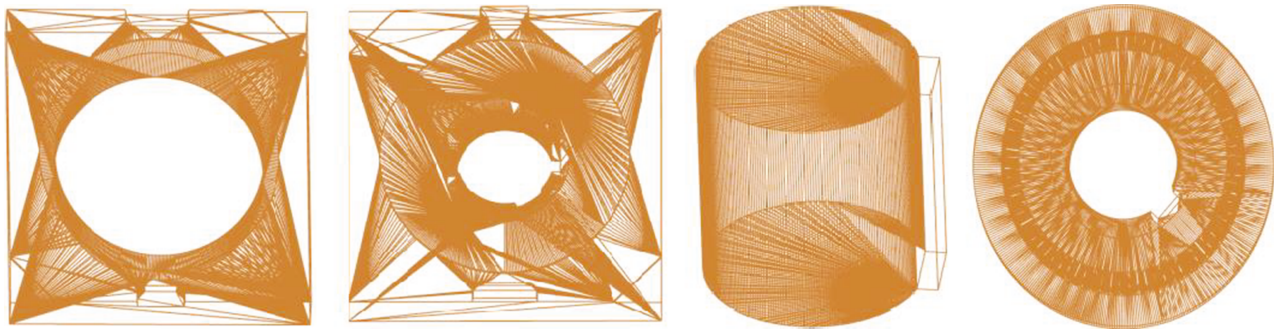

(a) Bottom die (b) Top die (c) Centre locating shaft (d) Core

Figure 5: The STL model of the spur face gear master mould.

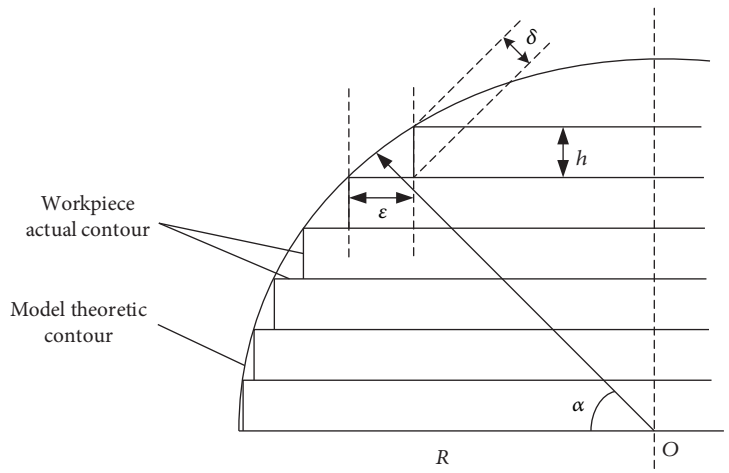

R: radius of a hemispherical model
h: layer thickness
a: the angle between the normal vector of a semisphere model surface and the piane of material accumulation (i.e.,, the forming direction of the semisphere surface model)

Figure 6: The local schematic of the "Step Effect" for forming parts.

parts is, and the more severe the "Step Effect" is when the α is constant, in view of α being a fixed value in the forming process. Thus, h should be taken as small as possible in the selection. At the same time, the selection of h is also limited by the nozzle diameter and forming efficiency of the rapid prototyping machine. Since the nozzle diameter of the BOX 3D rapid prototyping machine is 0.4 mm, the upper limit should be less than 0.4 mm to first determine the thickness of the layer; in order to reduce the influence of the "Step Effect" on the surface of the model, the layer thickness of 0.2 mm is selected next. In addition, according to Figure 6, an increase in the ε value and δ value of the forming parts' surface can also be obtained with the increase of the α value when the value of h is fixed. During the time when the value of α is zero, the "Step Effect" is at its minimum, while the "Step Effect" is at its largest when the value of α is ninety. As for the complex-shaped master mould of the spur face gear, there are many different shapes of the surface in the mould, so it is impossible to keep the forming direction of each mould surface at 0° with a high forming quality. For the sake of ensuring the quality of each critical surface involved in the wax injection process, it is necessary to minimize the forming direction α of this surface part. According to Figure 2, the surfaces of 4, 6, 8, 10, and 17 are critical surfaces, and the forming direction of the corresponding forming parts is shown in Figure 8.

3.2.2. Selection of Extrusion Speed and Filling Speed. Extrusion speed refers to the speed at which the forming material is extruded from the nozzle. Filling speed refers to the movement speed of the extruded wire to fill the filling trajectory.

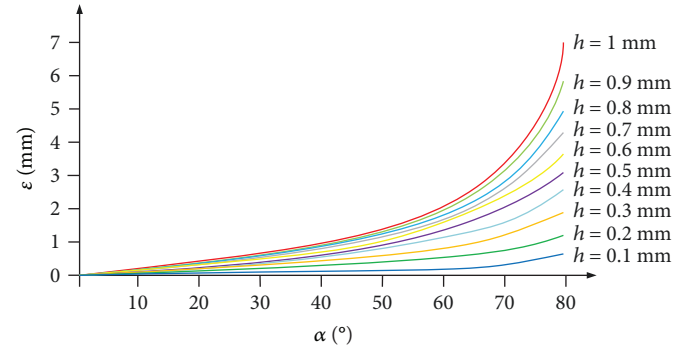

(a) The $\alpha - \varepsilon$ curves of different layer thicknesses

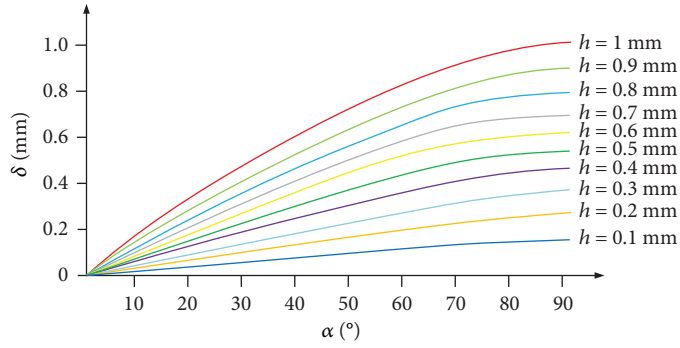

(b) The $\alpha - \delta$ curves of different layer thicknesses

FIGURE 7: The relation curves of $\alpha - \varepsilon$ and $\alpha - \delta$ on the surface of the forming parts are presented when $R = 100$ mm.

The amount of wire extruded from the nozzle in unit time will be much smaller than the amount of consumable material when the filling speed is much greater than the extrusion speed, which shall lead to the phenomenon of broken wires and parts difficult to form. The amount of wire extruded from the nozzle in unit time will be much larger than the amount of consumable material when the filling speed is much less than the extrusion speed, which will cause the excess molten wire to pile up on the sprinkler head that leads to each layer material distributed unevenly during forming, thus affecting the production quality [24]. To avoid the above problems, the amount of wire extruded from the nozzle during unit time shall be equal to the amount of consumable material used when filling, that is

$$v_j \times S_1 = v_t \times S_2, \tag{4}$$

where v_j is the extrusion speed, v_t is the filling speed, S_1 is the section area of the sprinkler head, and S_2 is the cross-sectional area of the wire in the process of filling. Since the shape of the nozzle cross section is approximately circular, thus

$$S_1 = \pi \times \left(\frac{d}{2}\right)^2, \tag{5}$$

where d refers to the diameter of the sprinkler head.

In the process of extrusion, the cross section of the wire is similar to that of the rectangular section due to the squeezing between layers and layers (as shown in Figure 9), and the sectional area S_2 is as follows:

$$S_2 = h \times p, \tag{6}$$

where p is the equivalent width of the filling wire section, which is slightly smaller than the actual width, and h refers to layer thickness.

Since the rapid prototyping machine controls the layer thickness by varying the screw speed, there is a corresponding relationship between them. In order to facilitate the study, it is assumed that the correspondence between them is a linear relation, and the linear regression equation $h = a' + b's$ of h with respect to s is solved by using maximum likelihood estimation. Then, the linear regression equation is solved in conjunction with (4), (5), and (6). So an expression between the speed of extrusion v_j and the filling speed v_t is concluded as follows:

$$v_j = \frac{4hb'v_t}{\pi d^2} \times s - \frac{4ha'v_t}{\pi d^2}. \tag{7}$$

In this paper, we took a cuboid of 10 mm × 5 mm × 5 mm as an example. The linear regression equation between the layer thickness h and the screw speed s of the BOX 3D rapid prototyping machine is $h = -0.22 + 0.004s$ based on the

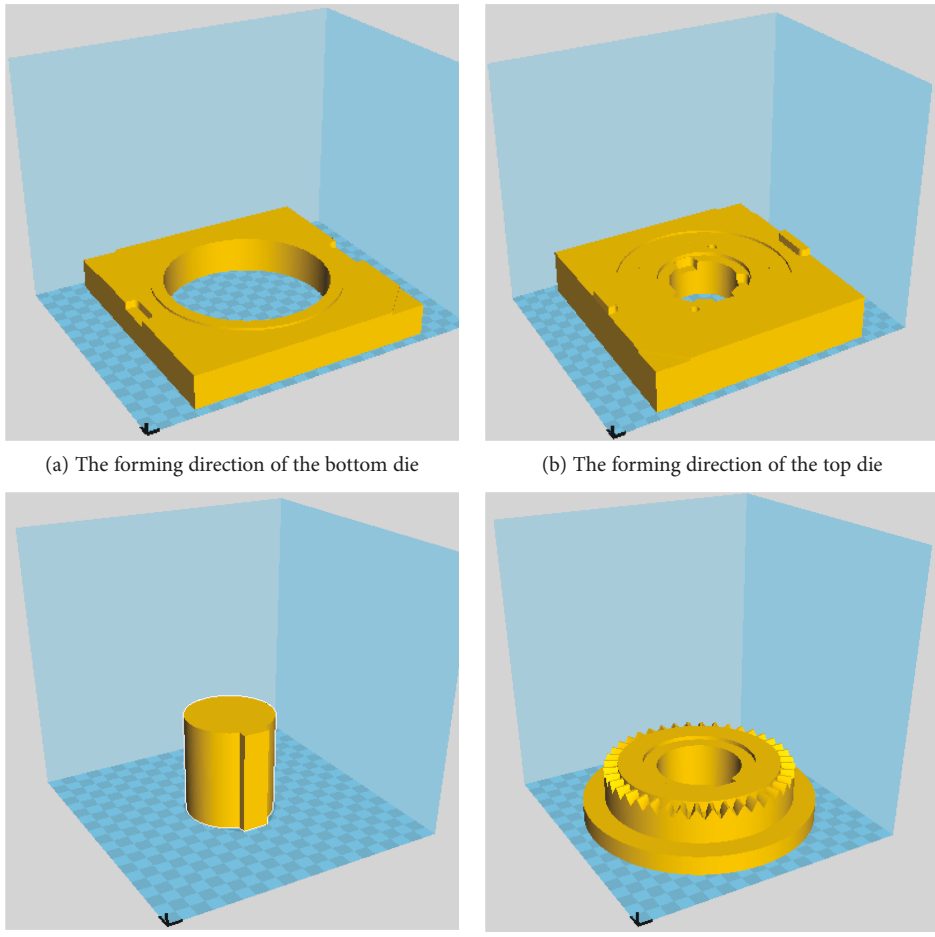

(a) The forming direction of the bottom die

(b) The forming direction of the top die

(c) The forming direction of the centre-locating shaft

(d) The forming direction of the core

Figure 8: Selection of the forming direction for the spur face gear master mould.

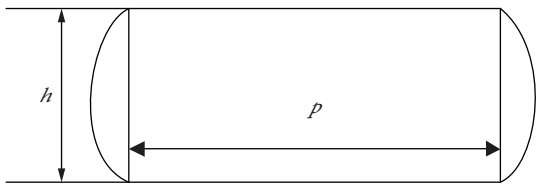

Figure 9: Cross section of the wire at filling.

different screw speeds that are shown in Table 5. When the filling speed v_t is selected, the document points out that the high filling speed will lead to less fluctuation stress during the forming process; the low filling speed will lead to a greater fluctuation of stress during the forming process, which will further cause fatigue effect and deformation of parts. Therefore, we determined that the filling speed v_t is 60 mm/s in this paper and the corresponding extrusion speed is 61.1 mm/s.

3.2.3. Selection of Nozzle Temperature and Ambient Temperature. Nozzle temperature refers to the temperature when the nozzle is heated, which determines the bonding property, accumulation performance, and flow capacity of the extruded wire; ambient temperature refers to the forming box temperature during the operation of the rapid prototyping machine, which determines the internal stress of the forming parts. The extruded wire will change from a molten state to a liquid with a small cohesion coefficient and high fluidity; when the nozzle temperature is too high, the next layer of wire material is piled up on the previous contour even if the shape has not been cooled and moulded, leading to the collapse and destruction of the previous layer and making it difficult to form the parts. When the nozzle temperature is too low, the extruded wire is in a semimolten state with a large cohesion coefficient and poor fluidity, which causes it not only to jam easily during extrusion, but also to crack between the lamellae. Furthermore, the overall strength of the formed parts is low because the temperature of the extruded wire is low and the bonding force between the layers and the filler material is very small. For ambient temperature, a high ambient temperature will help reduce the internal stress of the forming, but the surface of the forming parts is prone to wrinkling. The cooling speed of the extruded wire will be accelerated during the forming process if the ambient temperature is too low, and then the phenomenon of bonding and buckling of all the layers will occur as reported in

Table 5: The layer thickness measurement results of different screw speeds.

Screw speed s	100	110	120	130	140	150	160	170	180	190	200
Layer thickness h (mm)	0.18	0.22	0.26	0.30	0.34	0.38	0.42	0.46	0.50	0.54	0.58

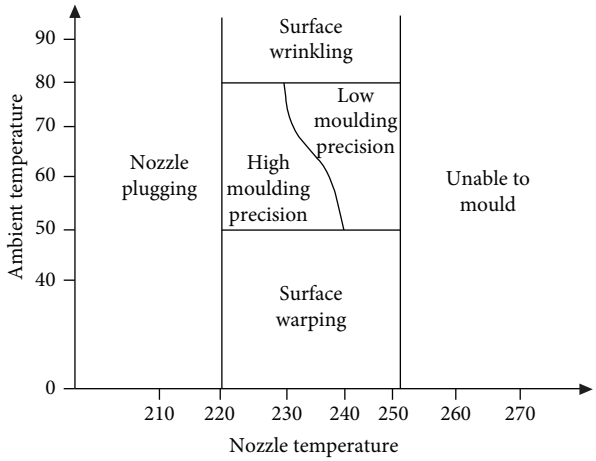

Figure 10: The reasonable ambient temperature range of different nozzle temperatures.

Table 6: Layered slice processing results of each model for spur face gear master mould.

Spur face gear master mould	Layer number of forming (layers)	Forming time	Consumption of ABS materials (g)
Centre-locating shaft	385	9 h 10 min	60
Core	305	11 h 6 min	238
Bottom die	150	6 h 40 min	92
Top die	219	8 h 23 min	136

[25]. Consequently, it is important to discuss the influence of different nozzle temperatures and ambient temperatures particularly on the quality of the moulded parts. Based on the large number of forming experiments performed on the 10 mm × 5 mm × 5 mm cuboid sample, the reasonable ambient temperature range at different nozzle temperatures is obtained (as shown in Figure 10). Meanwhile, the nozzle temperature and ambient temperature of the spur face gear master mould are 230°C and 60°C, respectively (Table 6).

3.2.4. Compensation Design of the Ideal Contour. The forming wire is extruded with a certain width when forming parts are produced by using the FDM rapid prototyping technology, and there is a distance between the actual contour line and the theoretical contour line when the nozzle is filled (as shown in Figure 11). The width of extruded forming wire is a variable due to the influence of extrusion speed, filling speed, layer thickness, and nozzle diameter, so it is necessary to establish a cross-sectional model of the extruded wire [26] (as shown in Figure 12), so as to make clear the quantitative

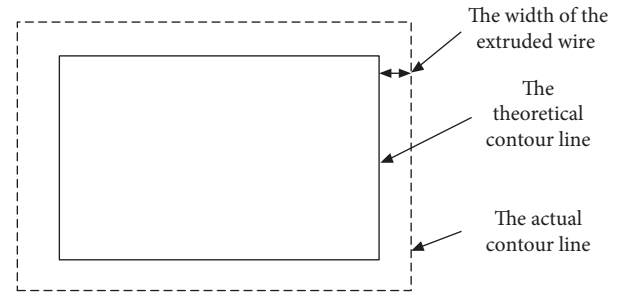

Figure 11: The error caused by the width of the extrusion wire.

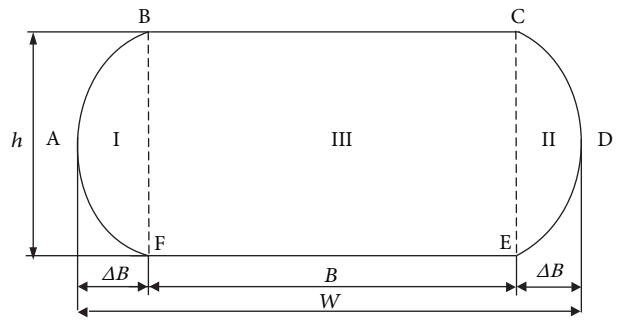

Figure 12: The sectional model of the extruded wire.

relationship between the extrusion width W and the technological parameters, in order to lay a theoretical foundation for the next step of postprocessing.

(1) The section of the extrusion wire can be simplified as area III in Figure 12 (i.e., the rectangular BCEF) when the extrusion speed is small and the corresponding extrusion wire width W is as follows:

$$W = B = \frac{\pi d^2}{4h}\frac{v_j}{v_t}. \tag{8}$$

(2) The section of the extrusion wire can be composed of areas I, II, and III in Figure 12 when the extrusion speed is large, and the corresponding extrusion wire width W is as follows:

$$W = B + 2\Delta B = B + 2 \times \frac{h^2}{2B} = \frac{B^2 + h^2}{B}, \tag{9}$$

where $B = (\lambda^2 - h^2)/2\lambda$, $\lambda = (\pi d^2/2h)(v_j/v_t)$, v_j is the

```
M127 TO
G0 F9000 X55. 919 Y56. 479 Z0. 300
; TYPE : SKIRT
G1 F1200 X56. 521 Y55. 909 E0. 01949
G1 X59. 930 Y52. 753 E0. 12873
G1 X60. 413 Y52. 342 E0. 14364
G1 X64. 143 Y49. 542 E0 .25330
G1 X64. 143 Y49. 543 E0. 25333
G1 X64. 888 Y48. 982 E0. 27526
G1 X65. 407 Y48. 601 E0. 29036
G1 X66. 240 Y48. 076 E0. 31355
G1 X70. 216 Y45. 687 E0. 42261
G1 X70. 808 Y45. 353 E0. 43860
G1 X71. 533 Y44. 994 E0. 45762
G1 X72. 064 Y44. 742 E0. 47144
G1 X76. 270 Y42. 773 E0. 58064
G1 X76. 856 Y42. 530 E0. 59555
G1 X81. 257 Y41. 000 E0. 70511
G1 X82. 100 Y40. 708 E0. 72609
G1 X82. 676 Y40. 515 E0. 74037
G1 X83. 705 Y40. 251 E0. 76535
G1 X88. 222 Y39. 185 E0. 87447
G1 X88. 856 Y39. 054 E0. 88970
G1 X89. 664 Y38. 937 E0. 90889
G1 X90. 269 Y38. 856 E0. 92325
G1 X94. 881 Y38. 260 E1. 03259
G1 X95. 512 Y38. 209 E1. 04748
```

(a) G code for the rapid prototyping of the core

```
M110
G0 F9000 X47. 901 Y47. 901 Z0. 300
;TYPE : SKIRT
G1 F1200 X252. 099 Y47. 901 E4. 80135
G1 X252. 099 Y252. 099 E9. 60270
G1 X47. 901 Y252. 099 E14. 40404
G1 X47. 901 Y47. 901 E19. 20539
G1 F2400 E14. 70539
G0 F9000 X51. 901 Y51. 901
;TYPE:WALL-INNER
G1 F2400 E19. 20539
G1 F1200 X248. 099 Y51. 901 E23. 81863
G1 X248. 099 Y248. 099 E28. 43187
G1 X51. 901 Y248. 099 E33. 04512
G1 X51. 901 Y51. 901 E37. 65836
G0 F9000 X126. 330 Y129. 142
G1 F1200 X123. 623 Y132. 692 E37. 76333
G1 X121. 444 Y136. 587 E37. 86827
G1 X119. 838 Y140. 752 E37. 97323
G1 X118. 849 Y145. 036 E38. 07661
G1 X118. 826 Y145. 131 E38. 07891
G1 X118. 462 Y149. 478 E38. 18148
G1 X118. 451 Y149. 577 E38. 18382
G1 X188. 705 Y154. 005 E38. 28811
G1 X119. 587 Y158. 398 E38. 39346
G1 X121. 068 Y162. 578 E38. 49773
G1 X123. 133 Y166. 535 E38. 60268
```

(b) G code for the rapid prototyping of the top die

```
M107
G0 F9000 X93. 262 Y90. 657 Z0. 300
; TYPE : SKIRT
G1 F1200 X98. 810 Y85. 810 E0. 17322
G1 X104. 770 Y81. 479 E0. 34646
G1 X111. 095 Y77. 701 E0. 51969
G1 X117. 731 Y74. 505 E0. 69287
G1 X124. 630 Y71. 916 E0. 86614
G1 X130. 737 Y70. 230 E1. 01510
G1 X131. 730 Y69. 955 E1. 03933
G1 X138. 980 Y68. 640 E1. 21258
G1 X145. 288 Y68. 073 E1. 36150
G1 X146. 316 Y67. 980 E1. 38577
G1 X153. 683 Y67. 980 E1. 55900
G1 X159. 995 Y68. 547 E1. 70801
G1 X161. 022 Y68. 640 E1. 73226
G1 X168. 269 Y69. 955 E1. 90544
G1 X174. 378 Y71. 641 E2. 05445
G1 X175. 371 Y71. 916 E2. 07868
G1 X182. 269 Y74. 505 E2. 25192
G1 X188. 905 Y77. 701 E2. 42511
G1 X195. 230 Y81. 479 E2. 59834
G1 X201. 190 Y85. 810 E2. 77157
G1 X206. 738 Y90. 657 E2. 94479
G1 X211. 829 Y95. 982 E3. 11802
G1 X216. 422 Y101. 742 E3. 29124
G1 X219. 910 Y107. 027 E3. 44013
```

(c) G code for the rapid prototyping of the bottom die

```
M112
G0 F9000 X113. 906 Y137. 570 Z0. 300
; TYPE : SKIRT
G1 F1200 X120. 842 Y137. 570 E0. 16309
G1 X121. 700 Y135. 394 E0. 21809
G1 X124. 072 Y131. 223 E0. 33091
G1 X126. 868 Y127. 611 E0. 43831
G1 X127. 001 Y127. 434 E0. 44352
G1 X130. 454 Y124. 087 E0. 55659
G1 X134. 149 Y121. 403 E0. 66397
G1 X134. 326 Y121. 270 E0. 66918
G1 X138. 578 Y119. 024 E0. 78225
G1 X143. 095 Y117. 403 E0. 89509
G1 X147. 795 Y116. 437 E1. 00791
G1 X152. 334 Y116. 160 E1. 11484
G1 X152. 589 Y116. 143 E1. 12085
G1 X157. 365 Y116. 532 E1. 23352
G1 X162. 045 Y117. 592 E1. 34635
G1 X166. 528 Y119. 304 E1. 45918
G1 X170. 752 Y121. 632 E1. 57203
G1 X174. 352 Y124. 381 E1. 67904
G1 X174. 555 Y124. 534 E1. 68502
G1 X177. 753 Y127. 764 E1. 79189
G1 X177. 932 Y127. 943 E1. 79784
G1 X180. 640 Y131. 593 E1. 90471
G1 X180. 793 Y131. 797 E1. 91070
G1 X183. 075 Y136. 011 E2. 02338
```

(d) G code for the rapid prototyping of the centre-locating shaft

Figure 13: The results of the stratified slice processing for the spur face gear model.

(a) Core (b) Bottom die (c) Top die

Figure 14: The parts forming the spur face gear master mould.

extrusion speed, d is the nozzle diameter, B is the width of the rectangular BCEF in area III, h is the layer thickness, and v_t is the filling speed.

According to Section 3.2.2, the extrusion speed v_j is 61.1 mm/s, which belongs to a situation when the speed of extrusion is greater. Thus, the width of the nozzle extrusion wire under the above process parameters is calculated as 0.68 mm in (9); that is, the actual dimension of the formed master mould is more than 0.68 mm of the theoretical size.

3.2.5. Rapid Prototyping of Spur Face Gear Master Mould. Based on the above discussion and analysis of seven important technological parameters that affect forming quality and forming efficiency in FDM rapid prototyping, each process parameter of the rapid prototyping spur face gear master mould is based on the settings by the BOX 3D rapid prototyping machine operation software, and each slice of the master model is processed by slicing in accordance with the subsequent set of forming process parameters, while the slicing results of each model and the corresponding G code for controlling the RP machine are obtained (as shown in Figure 13). Finally, the centre-locating shaft, core, bottom die, and top die are rapidly moulded by using this G code and the forming parts of the master mould for the spur face gear is obtained (as shown in Figure 14).

3.3. Analysis of Process Parameters of Spur Face Gear Master Mould in the Reprocessing Stage of Rapid Prototyping. In view of the characteristics of the FDM rapid prototyping technology, it is necessary to carry out the supporting, sanding, and polishing process for the formed parts in sequence. However, the model selected in this paper does not generate any external support structures during the forming process. Therefore, only sanding and polishing are performed here. First of all, the purpose of the sanding process is to compensate for the errors caused by the extrusion nozzle wire width and to eliminate the "Step Effect" of each formed parts so as to meet the assembling accuracy requirements [27, 28]. Secondly, in order to further improve the surface

Table 7: The final postprocessing results of the spur face gear master mould.

	Measurement object (critical surface)	Theoretical value	Actual measurement value	Error	Roughness
4	Diameter of the cylindrical die cavity	137.700 mm	137.610 mm	0.090 mm	$R_a = 0.007\ \mu$m
	Height of the cylindrical die cavity	30.000 mm	30.111 mm	0.111 mm	
6	Surface of the reflexive mould of the spur face gear	—	—	0.083 mm	$R_a = 0.01\ \mu$m
	Inner diameter of the reflexive mould of the spur face gear	117.402 mm	117.460 mm	0.058 mm	
	External diameter of the reflexive mould of the spur face gear	137.40 mm	137.482 mm	0.082 mm	
	Height of the reflexive mould of the spur face gear	8.886 mm	8.956 mm	0.070 mm	
8 cores	Inner diameter of the keyway pouring cavity	65.888 mm	65.852 mm	0.036 mm	
	Outer diameter of the keyway pouring cavity	81.600 mm	81.526 mm	0.074 mm	
	Height of the keyway pouring cavity	3.061 mm	3.152 mm	0.091 mm	
8 top dies	Inner diameter of the keyway pouring cavity	65.988 mm	65.900 mm	0.088 mm	
	External diameter of the keyway pouring cavity	81.600 mm	81.520 mm	0.080 mm	
	Height of the keyway pouring cavity	3.061 mm	3.138 mm	0.077 mm	
10	External diameter of the centre-locating shaft	65.688 mm	65.750 mm	0.062 mm	$R_a = 0.0075\ \mu$m
17	Diameter of the cylindrical groove	158.000 mm	158.181 mm	0.181 mm	$R_a = 0.01\ \mu$m
	Height of the cylindrical groove	2.000 mm	2.069 mm	0.069 mm	
1	Length of the square base	197.700 mm	198.022 mm	0.322 mm	$R_a = 0.007\ \mu$m
	Height of the square base	28.000 mm	28.245 mm	0.245 mm	
5	Outer diameter of the cylindrical boss	157.700 mm	158.067 mm	0.121 mm	
	Height of the cylindrical boss	30.000 mm	30.192 mm	0.192 mm	
7	Diameter of the cylindrical base	169.700 mm	170.043 mm	0.343 mm	$R_a = 0.01\ \mu$m
	Height of the cylindrical base	14.000 mm	14.247 mm	0.247 mm	
9	Diameter of the centre-locating hole	65.888 mm	65. 781 mm	0.107 mm	
	Height of the centre-locating hole	36.860 mm	36.973 mm	0.113 mm	
11	Length of the square base	197.700 mm	197.950 mm	0.250 mm	
	Height of the square base	35.060 mm	35.233 mm	0.173 mm	
13	Height of the centre-locating hole	30.000 mm	30.312 mm	0.312 mm	

roughness and smoothness of the polished parts, mechanical polishing is used to polish the surface of the forming parts. Finally, the final postprocessing results are shown in Table 7 according to the postprocessing process shown in Figure 15.

As it is shown in Table 5, the dimension accuracy of the master mould critical surface ranges from 0.036 mm to 0.181 mm, the dimension accuracy of the noncritical surface ranges from 0.107 mm to 0.343 mm, and the surface roughness of the master mould is within the range of 0.007–0.01 μm. Thus, the forming parts of the spur face gear master mould have a higher quality precision and surface smoothness.

4. Construction of FDM Rapid Prototyping Process Model for Spur Face Gear Master Mould

In order to establish the mathematical model of the FDM rapid prototyping complex-shaped mould according to the data relationship between the forming parameters and moulding quality in each process stage, this paper adopts the method of stepwise regression analysis. Using the F significance test, the influence of the above process parameters on the forming quality is determined firstly, and then the corresponding mathematical model is solved by combining the linear regression equation. It is found that the quantitative relationship between the forming parameters of rapid prototyping and the forming quality is as follows:

$$y = AS_L^{b_0} h^{b_1} \alpha^{b_2} v_t^{b_3} T^{b_4} t^{b_5}, \tag{10}$$

where y denotes the forming accuracy and A, b_0~b_5 denotes the regression equation coefficient of the FDM rapid prototyping complex-shaped mould (related to the structure and process of forming parts, etc.)

Therefore, using the above big data process parameter model, this paper verifies and compares the spur face gear master mould manufactured by this technology with the traditional milling mould. The results are as shown in Table 8.

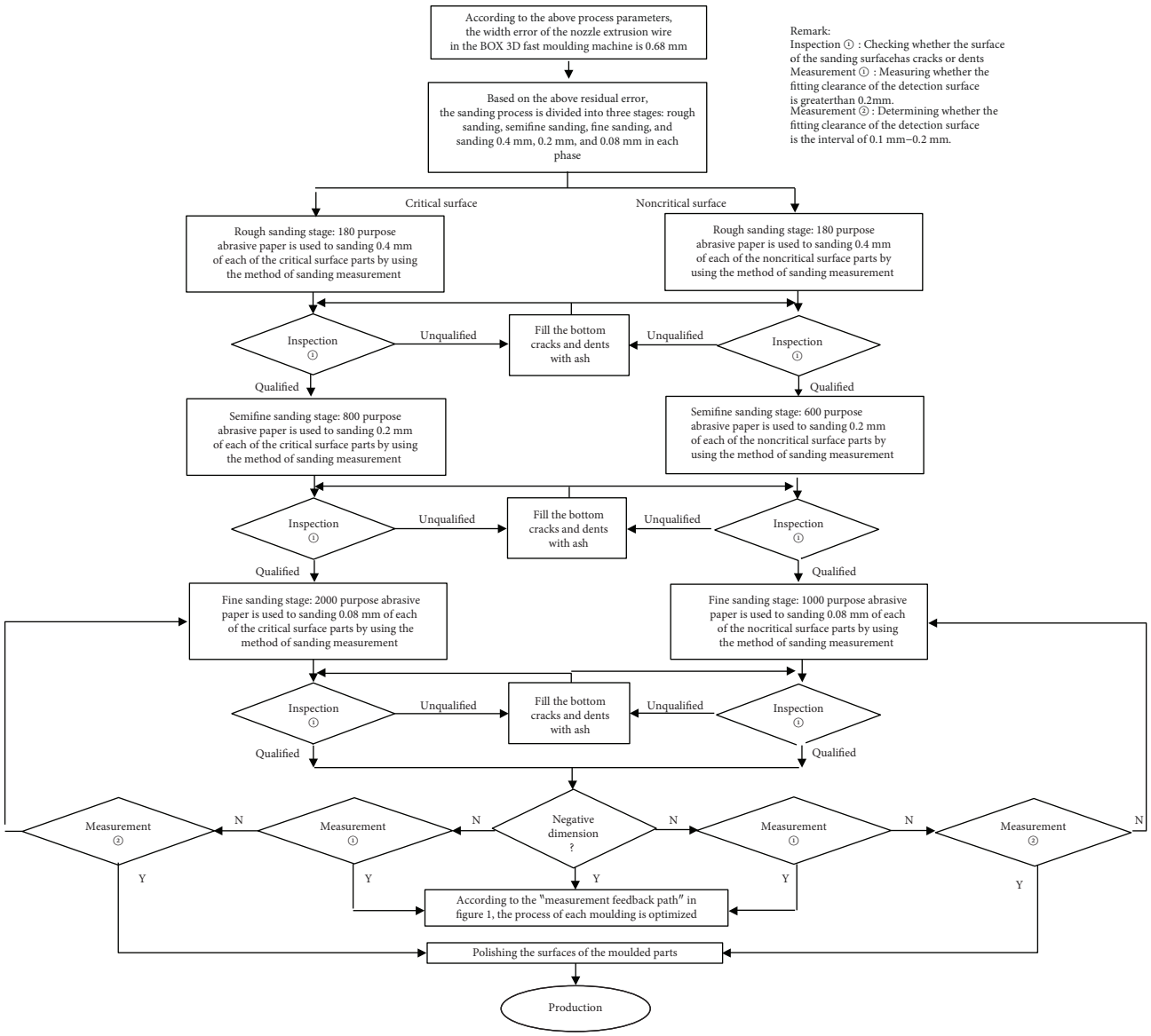

Figure 15: The postprocessing flow chart for the spur face gear master mould.

Table 8: Comparison of two processing methods for manufacturing spur face gear master mould.

Processing mode	Processing cycle (days)	Processing cost (dollars)	Forming quality	
			Machining accuracy (mm)	Machining roughness (μm)
Subtractive material manufacturing	7–10	300	0.02–0.05 mm	<0.01 μm
Additive material manufacturing	1-2	100	0.036 mm–0.181 mm	0.007–0.01 μm

5. Conclusion

Based on the FDM rapid prototyping technology of the spur face gear master mould, firstly, the mechanism of the preprocessing of the three-dimensional model of the mould in magnification and shell extraction is studied from the point of view of the material forming characteristics, and combined with the STL model conversion algorithm, the theoretical analysis of the preprocessing is realized. Secondly, from the angle of the forming and spraying mechanism of the forming materials and the quantitative relationship between each forming process parameter and forming quality, the forming

efficiency is studied, and the postprocessing technology of the FDM rapid prototyping mould based on this relation is put forward. Finally, according to the measurement results of the workpiece, the reasonableness of big data extraction and mathematical expression in the FDM rapid prototyping process is verified. Thus, it lays a solid theoretical foundation and data guarantee for the construction of the rapid prototyping process system based on cloud manufacturing data management, so that it can better carry on the technology docking.

Data Availability

The data used to support the findings of this study are available from the corresponding author upon request.

Conflicts of Interest

The authors declare that there are no conflicts of interest regarding the publication of this article.

Acknowledgments

This paper is supported by the National Natural Science Foundation of China (Grant no. 51705392), the Key Laboratory Scientific Research Project of Shaanxi Education Department (Grant no. 17JS058), and An Open Fund Project of Shaanxi Special Processing Key Laboratory in 2017 (Grant no. 2017SXTZKFJG04).

References

[1] J. Luo, Y. Guo, and X. Wang, "Rapid fabrication of curved microlens array using the 3D printing mold," *Optik*, vol. 156, pp. 556–563, 2018.

[2] E. Maneas, W. F. Xia, and D. I. Nikitichev, "Anatomically realistic ultrasound phantoms using gel wax with 3D printed mould," *Physics in Medicine & Biology*, vol. 63, no. 1, pp. 416–421, 2018.

[3] M. Upadhyay, T. Sivarupan, and M. El Mansori, "3D printing for rapid sand casting—a review," *Journal of Manufacturing Processes*, vol. 29, pp. 211–220, 2017.

[4] J. W. Kang and Q. X. Ma, "The role and impact of 3D printing technologies in casting," *China Foundry*, vol. 14, no. 3, pp. 157–168, 2017.

[5] X. Liu and W. Fan, "Study on data segmentation technique of large rapid prototyping workpiece based on features," *Tool Engineering*, vol. 45, no. 11, pp. 52–54, 2011.

[6] S. Huang, X. Gu, H. Zhou, and Y. Chen, "Two-dimensional optimization mechanism and method for on-demand supply of manufacturing cloud service," *Computers & Industrial Engineering*, vol. 117, pp. 47–59, 2018.

[7] J. Y. Lee, J. S. Yoon, and B. H. Kim, "A big data analytics platform for smart factories in small and medium-sized manufacturing enterprises: an empirical case study of a die casting factory," *International Journal of Precision Engineering and Manufacturing*, vol. 18, no. 10, pp. 1353–1361, 2017.

[8] L. Guo and J. Qiu, "Combination of cloud manufacturing and 3D printing: research progress and prospect," *International Journal of Advanced Manufacturing Technology*, vol. 96, no. 5–8, pp. 1929–1942, 2018.

[9] C. Yu, S. Mou, Y. Ji, X. Xu, and X. Gu, "A delayed product differentiation model for cloud manufacturing," *Computers & Industrial Engineering*, vol. 117, pp. 60–70, 2018.

[10] X. B. Li and Y. Chao, "Cloud services oriented manufacturing execution system for production process," *Computer Integrated Manufacturing Systems*, vol. 22, no. 1, pp. 178–188, 2016.

[11] Z. Liu, Y. Wang, L. Cai, Q. Cheng, and H. Zhang, "Design and manufacturing model of customized hydrostatic bearing system based on cloud and big data technology," *The International Journal of Advanced Manufacturing Technology*, vol. 84, no. 1–4, pp. 261–273, 2016.

[12] S. H. Xia, Y. Q. Shi, S. Wu, and B. Z. Chen, "Research on virtual resources scheduling for multi-objective optimization in cloud manufacturing environment," *Application Research of Computers*, vol. 36, no. 6, pp. 1–4, 2018.

[13] H. L. Yang, S. G. Tong, and R. R. Wu, "Automation technology of injection mold design based on case-based reasoning," *Chinese Journal of Mechanical Engineering*, vol. 44, no. 10, p. 288, 2008.

[14] A. Xu, "Design of multi direction synchronous core pulling mould for bearing ring," *Plastic Science and Technology*, vol. 46, no. 1, pp. 85–89, 2018.

[15] O. A. Mohamed, S. H. Masood, and J. L. Bhowmik, "Experimental investigation of time-dependent mechanical properties of PC-ABS prototypes processed by FDM additive manufacturing process," *Materials Letters*, vol. 193, pp. 58–62, 2017.

[16] J. Zhang, B. Yang, F. Fu, F. You, X. Dong, and M. Dai, "Resistivity and its anisotropy characterization of 3D-printed acrylonitrile butadiene styrene copolymer (ABS)/carbon black (CB) composites," *Applied Sciences*, vol. 7, no. 1, 2017.

[17] T. M. Wang, J. T. Xi, and H. Jin, "Prototype warp deformation in the FDM process," *Chinese Journal of Mechanical Engineering*, vol. 42, no. 03, pp. 233–238, 2006.

[18] Z. Y. Zhang, P. Chen, and L. Yang, "The subdivision algorithm of STL model with low precision in rapid prototyping process," *Journal of Mechanical Engineering*, vol. 52, no. 7, pp. 178–186, 2016.

[19] H. Q. Zhou and J. J. Wu, "New optimization method of STL model slice contour on rapid prototyping," *Journal of Manufacturing Automation*, vol. 37, no. 6, pp. 25–27, 2015.

[20] J. S. Chohan and R. Singh, "Pre and post processing techniques to improve surface characteristics of FDM parts: a state of art review and future applications," *Rapid Prototyping Journal*, vol. 23, no. 3, pp. 495–513, 2017.

[21] J. Singh, R. Singh, and H. Singh, "Investigations for improving the surface finish of FDM based ABS replicas by chemical vapor smoothing process: a case study," *Assembly Automation*, vol. 37, no. 1, pp. 13–21, 2017.

[22] O. A. Mohamed, S. H. Masood, and J. L. Bhowmik, "Mathematical modeling and FDM process parameters optimization using response surface methodology based on Q-optimal design," *Applied Mathematical Modelling*, vol. 40, no. 23-24, pp. 10052–10073, 2016.

[23] Y. X. Gong, C. Chen, M. X. Xia, and E. Q. Song, "Step effect analysis of FDM 3D printing model surface," *Journal of Mechanical Transmission*, vol. 4, no. 3, pp. 27–30, 2016.

[24] Y. Tlegenov, Y. S. Wong, and G. S. Hong, "A dynamic model for nozzle clog monitoring in fused deposition modelling," *Rapid Prototyping Journal*, vol. 23, no. 2, pp. 391–400, 2017.

[25] T. M. Wang, H. Jin, and J. T. Xi, "The adhesive mechanism and thermal analysis of fibers in the FDM process," *Journal of Shanghai Jiaotong University*, vol. 40, no. 7, pp. 1231–1238, 2017.

[26] M. W. M. Cunico, M. M. Cunico, P. M. Cavalheiro, and J. de Carvalho, "Investigation of additive manufacturing surface smoothing process," *Rapid Prototyping Journal*, vol. 23, no. 1, pp. 201–208, 2017.

[27] X. Jin, "Study of chemical post-processing method for fused deposition modeled three-dimensional printing materials," *Transactions of The Korean Society of Mechanical Engineers*, vol. 41, no. 9, pp. 839–844, 2017.

[28] K. Salonitis, L. D'Alvise, B. Schoinochoritis, and D. Chantzis, "Additive manufacturing and post-processing simulation: laser cladding followed by high speed machining," *International Journal of Advanced Manufacturing Technology*, vol. 85, no. 9-12, pp. 2401–2411, 2016.